LATERAL DYNAMICS SIMULATION OF WEBS HAVING CROSS-MACHINE DIRECTION VARIATION

By

Stephen Lange, Michael Looney, and Jeremy Carrle
Procter & Gamble
USA

ABSTRACT

Webs often include sectional variation in caliper or modulus of elasticity as a result of undesirable manufacturing variation or by intentional design. These variations influence wrinkle formation and tracking control in multi-span web handling systems. This paper shares the results of finite element simulations of the lateral dynamics of webs having variation in thickness and modulus in cross-machine direction. Span length and machine-direction bulk strain were varied and the effects on lateral steering and wrinkle formation were simulated for a variety of inhomogeneous webs.

Key variables affecting the lateral steering include the CMD location of the thick section and its width, the stiffness of the thick section, the z-direction bias of the thick section relative to the roller surface, the average strain in the composite web and the span length/width ratio. The web shifted in most cases toward the half of the web having the thick section, though not all. The combination of a web with a thick, stiff section having a width 1/10-1/6 that of the base web, coincident with the web edge, in long spans with low strain generated the largest lateral shift. Wrinkles were generated for some conditions where the thick section was located on or near web centerline.

NOMENCLATURE

d_{op}	lateral shift of operator side web edge at downstream roller, mm
d_{dr}	lateral shift of drive side web edge at downstream roller, mm
E	Young's Modulus of the base web, GPa
E_s	Young's Modulus of the thick section of the web, GPa
h	base web thickness, mm
L	span length, mm
W	total unstrained web width, mm
Δw	change in web width from entry to span to exit of span, mm
R	roller radius, mm
s	section width, mm

t	section thickness, mm
z	section offset from the base web neutral axis, mm
V	web velocity, m/s
y	cross-direction center-to-center distance of strip to base web, mm
ε_{md}	nominal machine direction strain
μ_s	static coefficient of friction between rollers and web

INTRODUCTION

Variation in web properties such as thickness or modulus of elasticity is ubiquitous due to normal and special cause variation in the processes used to manufacture webs, both in machine and cross-machine directions. For example, gauge bands in cast films due to die imperfections or variation in fiber laydown distribution in nonwovens are two such cases.

In some products, webs are combined intentionally to create a web that results in machine and cross-machine direction variation, for example when a continuous strip or a discrete patch of one web is laminated to a wider carrier web or a coating is applied in sections or intermittently.

Web wrinkling and mistracking (excessive lateral shifts) can often be caused by either web or roller nonuniformity or misalignment. Closed form analytical equations, finite element modeling, and empirical studies have been used to understand the effects of some cases of roller and/or web nonuniformity on web behavior. Beisel [1], [2] studied the effects of misaligned, tapered and crowned rollers on trough and wrinkle formation. Good, et al, [3] extended the work to orthotropic webs and prediction of wrinkles due to holes in webs. Swanson [4] explored the effects of cambered webs on tracking and wrinkling.

This paper focuses on the effects of a web containing a single continuous, machine-direction oriented section having different properties than the base web on web tracking and wrinkling in interaction with a series of two idler rollers. The analysis was executed using a Space-Filling experimental design comprised of 100 finite element computer simulation runs (see Appendix).

WEB AND PROCESS VARIABLES

The simulated web path included two 90 mm diameter idler rollers with a wrap angle of 180 degrees (Figure 1). The span length between the idler rollers was varied in the simulation.

In the simulations, the web's inhomogeneity was simulated by increasing its thickness and z-direction position of the thickness in a continuous section. This section was varied by changing its width, s, cross-machine location relative to the base web centerline, y, thickness, t, and offset position, z, relative to the neutral axis of the base web (Figure 2). The section's Young's Modulus was also varied. Web and section materials are assumed isotropic with Poisson's ratio of 0.3.

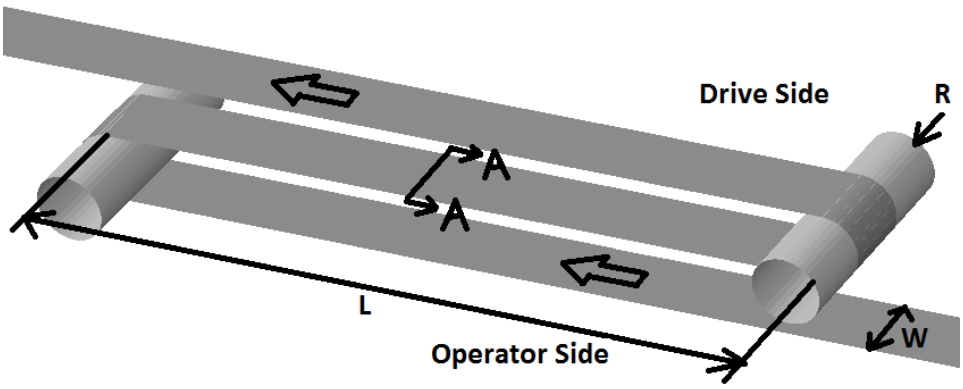

Figure 1 – Web path layout for simulation

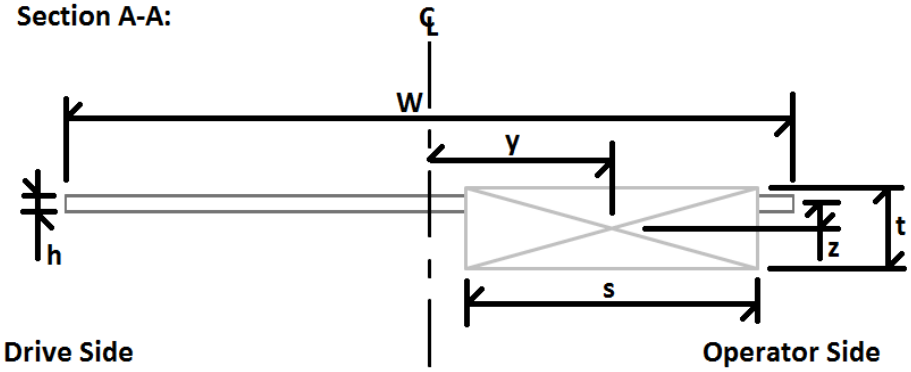

Figure 2 – Cross-section of Simulated Web with a Thick Section

Parameters	Value
E (GPa)	0.1
h (mm)	0.1
W (mm)	100
R (mm)	45
V (m/s)	~1
μ_s	0.8
Variables	**Range**
ε_{md}	0.005-0.020
E_s (GPa)	0.1-0.5
L (mm)	100-1000
s (mm)	5-50
t (mm)	0.1-0.5
y (mm)	0-47.5
z (mm)	-0.2-0.2

Table 1 – Simulation Parameters and Variable Ranges

Simulation Computational Parameters

Dassault Systèmes' ABAQUS/Explicit version 6.12 software was used as the finite element analysis tool. Simulation time for each run was approximately 6 seconds to allow steady state mistrack conditions to be achieved at the downstream roller. Shell elements with a mesh size of 5 mm were used.

To prevent premature steering and wrinkling on the upstream roller with the long entry span needed for the simulation, the web was constrained laterally down its machine direction centerline in the entry span to 90 degrees of wrap on the upstream roller. It was again constrained laterally down its machine direction centerline close to the tangent point of the exit of the downstream roller.

RESULTS

For most simulation runs the web shifted laterally toward the operator side of the web which contained the non-uniform thick section. If the thick section was more centered on the base web, generally there was a smaller lateral shift. In a small set of runs, the web shifted in the opposite direction (see Table 5).

A selection of the simulation runs having the largest lateral shift of the operator side edge of the web, $d_{op,}$ is shown in Table 2. Data for the other web edge deflection, d_{dr}, are virtually identical and are included in the Appendix.

Run	s	t	E_S	L/W	ε_{md}	y	z	d_{op}
8	10	0.5	0.9	8.2	0.007	15	-0.2	1.59
12	40	0.5	0.4	8.7	0.005	25	-0.1494	2.31
22	5	0.49	0.5	5.5	0.02	47.5	0.19344	1.79
67	15	0.43	1	10	0.005	42.5	0	7.49
75	35	0.38	0.5	7.2	0.005	32.5	0.14	3.10
94	10	0.49	1	10	0.016	45	-0.195	2.19
97	50	0.5	0.2	9.4	0.017	25	0.2	2.53

Table 2 – Simulation Runs with Largest Lateral Shift

These runs tend to have the thickest sections (>0.38 mm), higher span lengths to web width ratios, L/W (>5.5) and the thick section displaced laterally from the web's machine direction centerline (y>15 mm).

Table 3 includes simulation runs having the least amount of lateral shift on the operator side edge of the web.

Run	s	t	E_s	L/W	ε_{md}	y	z	d_{op}
4	40	0.17	0.9	1	0.008	10	-0.03402	0.0008
5	50	0.1	0.1	6.3	0.017	0	0	0.0003
25	50	0.1	0.1	9.9	0.005	25	0	0.0003
51	10	0.1	0.8	8.6	0.005	0	0	0.0008
62	50	0.1	0.1	10	0.02	0	0	0.0004
69	30	0.1	0.9	10	0.005	0	0	0.0002
78	10	0.1	0.1	10	0.02	0	0	0.0004
90	20	0.1	1	1	0.01	0	0	0.0009
93	10	0.1	0.7	5.1	0.02	0	0	0.0006

Table 3 – Simulation Runs with Minimum Lateral Shift

These runs generally include webs that do not have a thick section relative to the base web (t=0.1 and z=0), i.e. they have dimensional uniformity and have only variation in modulus of the non-uniform section.

L/W Effect

Figures 3, 4, and 5 are contour plots of d_{op} versus the cross-machine shift, y, of the non-uniform section, the thickness of the nonuniform section, t, and the bias of the thick section from the base web's neutral axis, z with L/W, respectively.

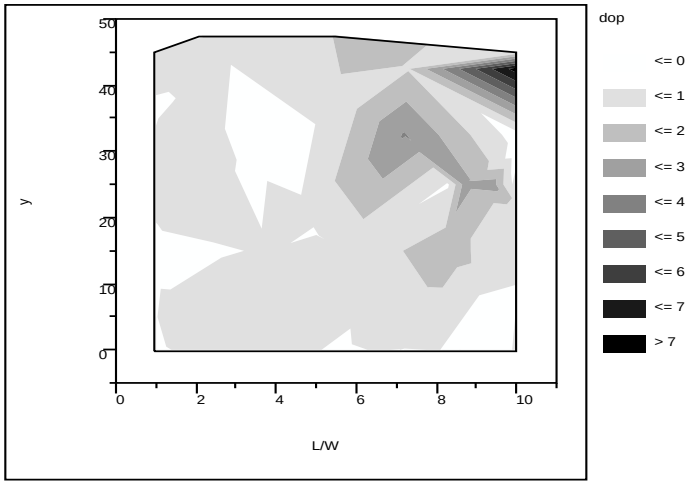

Figure 3 – d_{op} versus y and L/W

The largest lateral shifts occur with longer span length/width ratios and greater cross-direction shifts from web centerline of the thick section.

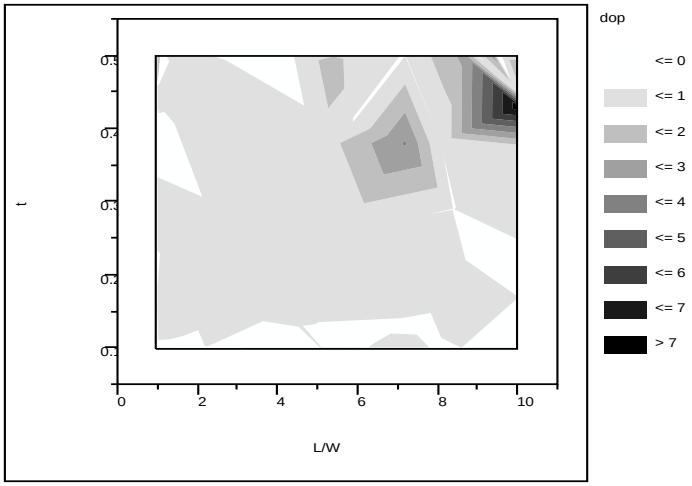

Figure 4 – d_{op} versus t and L/W

The largest lateral shifts occur with the largest L/W's for the webs having the thickest section, t.

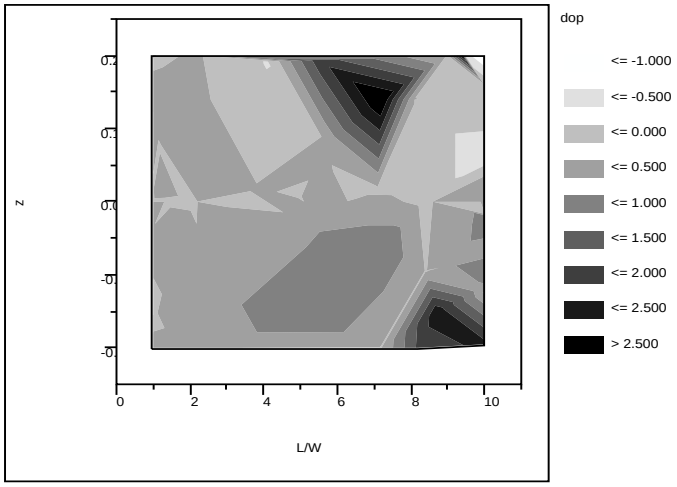

Figure 5 – d_{op} versus z and L/W

The largest lateral shifts occur with the largest L/W's and the extremes of the z direction offset of the thick section (-0.2 and 0.2 mm), with a larger region associated with the configuration where the thick section is against the roller (z=0.1-0.2 mm).

Strain Effect

Figures 6, 7, and 8 show plots of d_{op} versus ε_{md} and t, y, and z, respectively.

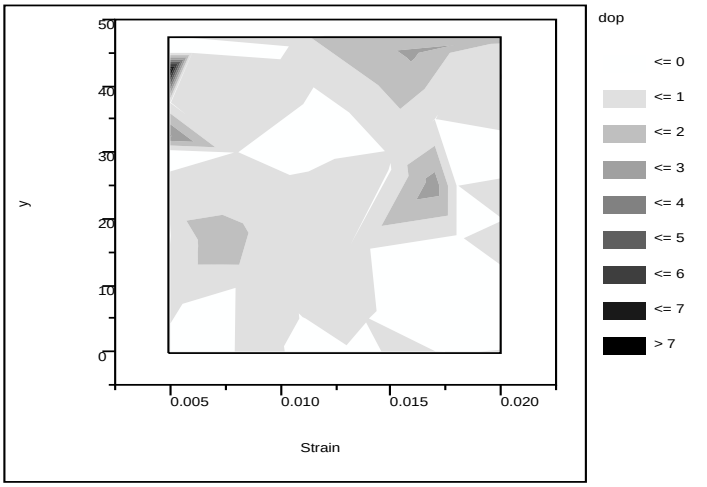

Figure 6 – d_{op} versus ε_{md} and y

The largest lateral shifts occur with the smallest strain and largest y combination.

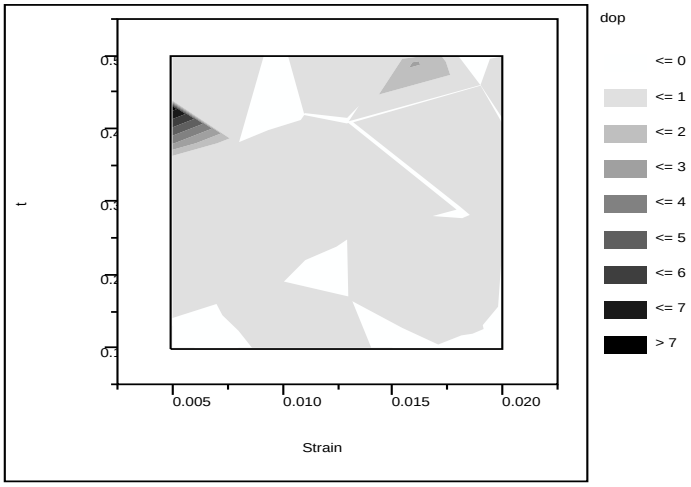

Figure 7 – d_{op} versus t and ε_{md}

The largest lateral shift occurs at the combination of smallest strain (~0.005) and larger thickness section (t~0.4).

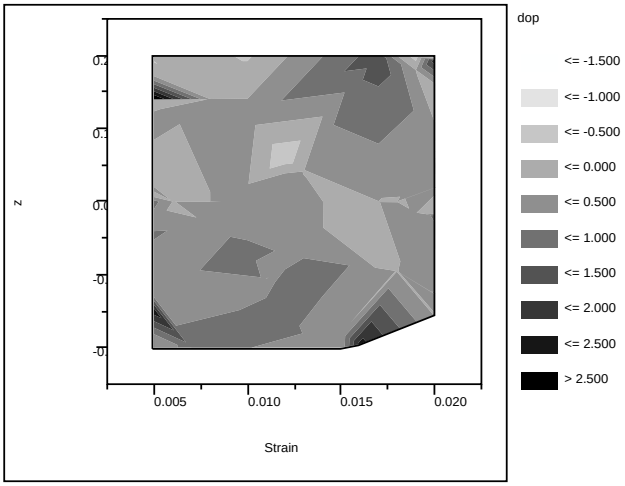

Figure 8 – d_{op} versus z and ε_{md}

Larger lateral shifts are found at combinations of the extreme z (positive and negative) and extreme strains (0.005 and ~0.016).

Modulus Effect

The modulus of the non-uniform section is plotted with t, y, and z versus d_{op} in Figures 9, 10, and 11.

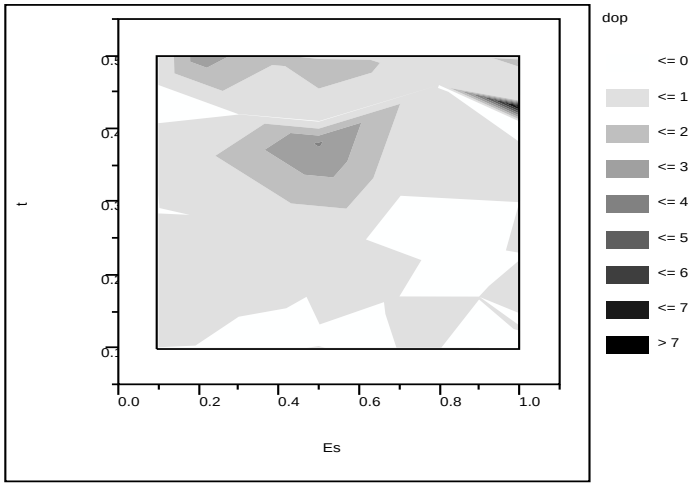

Figure 9 – d_{op} versus t and E_s

Webs simulated with stiffer sections (a combination of higher modulus and thickness) exhibit the largest lateral shifts.

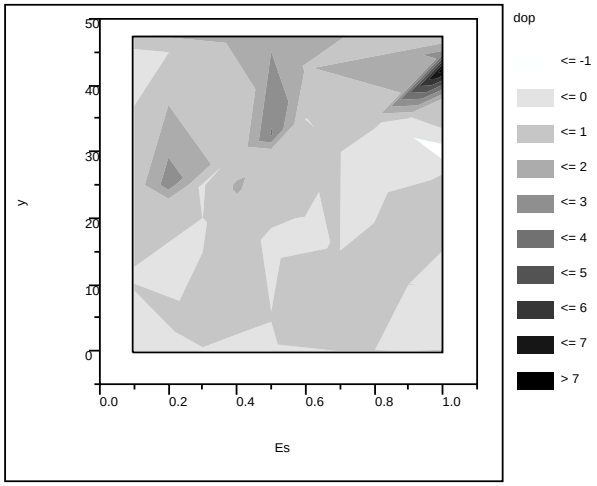

Figure 10 – d_{op} versus y and E_s

Combinations of large modulus sections combined with a cross direction shift off machine centerline result in the largest lateral shifts.

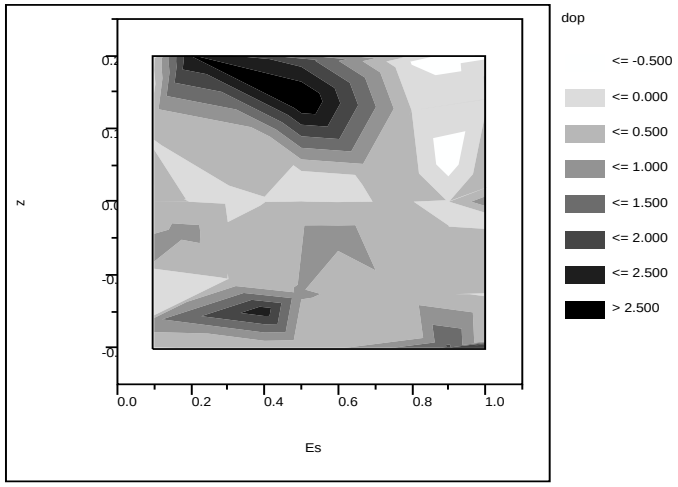

Figure 11 – d_{op} versus z and E_s

Both large and small z-displacements of the thick section result in larger shifts. At combinations of high modulus and positive z displacement, the web shifts in the negative direction.

Section Width Effect

Figures 12, 13 and 14 show plots of d_{op} versus the section width, s with t, y, and z, respectively.

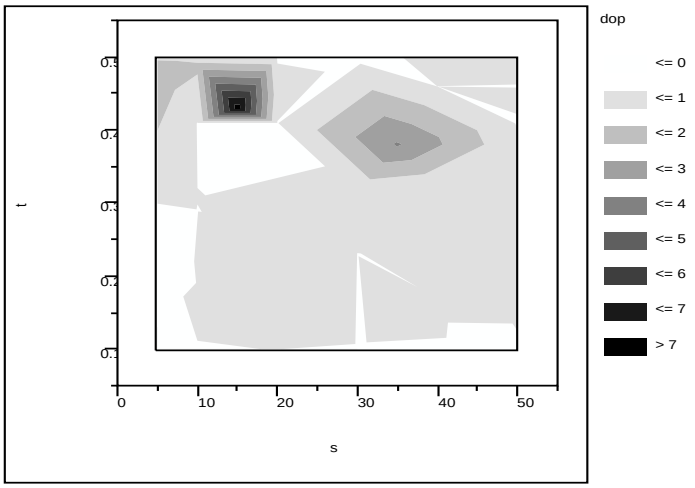

Figure 12 – d_{op} versus t and s

The largest lateral shifts occurred with combinations of section widths of 10-20 mm and at higher thicknesses (>0.4 mm).

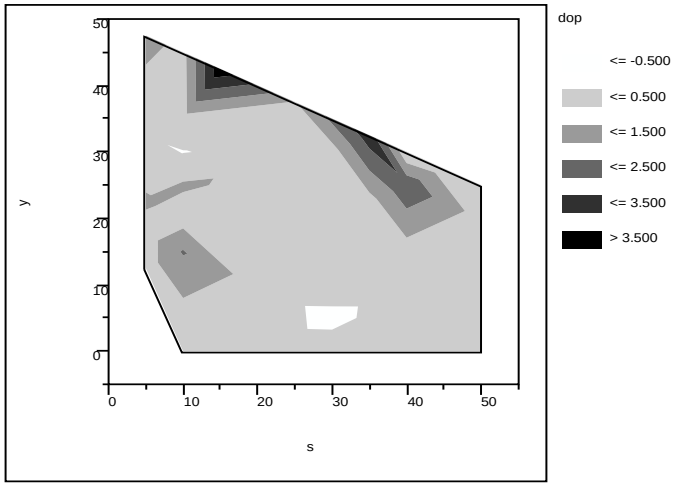

Figure 13 – d_{op} versus y and s

A broad range of section widths combined with a lateral position off web centerline provided the highest lateral shifts. The surface appears cut off because configurations where the section would have extended beyond the base web edge were not included in the simulation. For example, a section width of 50 mm can't be located more than 25 mm off the base web centerline without extending beyond the edge.

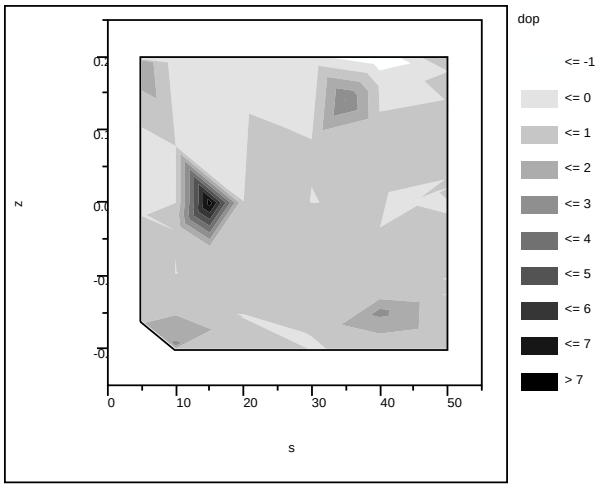

Figure 14 – d_{op} versus z and s

The largest lateral shifts were at combinations of section widths of 10-20 mm and essentially symmetric distribution of extra thickess about the base web's neutral axis (see related runs in Table 4 and Figure 15).

Extreme Case Simulations

After completing the 100 simulations, additional simulation runs were completed at conditions expected to give maximum lateral shifting based on key variables identified

from the simulation. Only the section width, s was varied, keeping its outboard edge fixed to the web edge. Table 4 shows the simulation conditions and the result and Figure 15 shows a schematic (not to scale) of the web cross-section for each run and a plot of the web mistrack:

t	E_s	L/W	ε_{md}	z
0.5	1	10	0.005	0.2

Table 4 – Maximum Lateral Shift Common Conditions

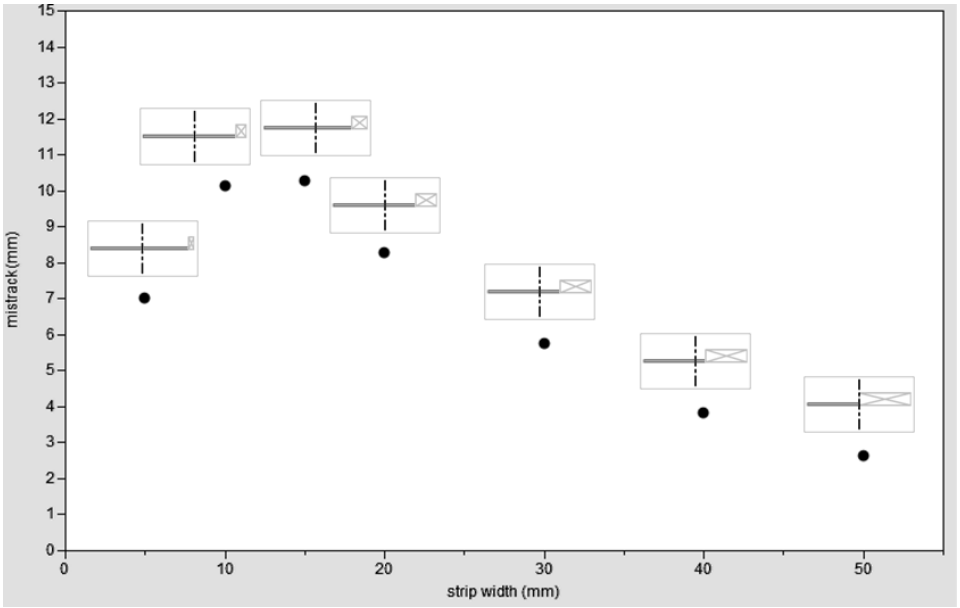

Figure 15 – Schematic of Web Configurations and Associated Mistrack

Interestingly, for this set of conditions there is a section width approximately 1/10-1/6 of the base web width where the lateral shift is maximized. Note that as s approaches 0 or W, the lateral shift is expected to also approach 0, as the web becomes substantially uniform.

Negative Direction Lateral Shift

The following runs in Table 5 tracked over significantly not to the operator side of the web with the thick section, but rather to the drive side.

Run	s (mm)	t (mm)	E_s (GPa)	L/W	ε_{md}	y (mm)	z (mm)	Δw (mm)	d_{op} (mm)	d_{dr} (mm)
19	30	0.50	0.9	9.5	0.019	5	0.1994	-0.19	-0.77	-0.58
21	40	0.50	1.0	10	0.02	30	0.2	-0.14	-1.84	-1.70
39	5	0.22	0.9	10	0.012	32.5	0.06	-0.018	-0.86	-0.84
56	10	0.50	0.8	4.1	0.005	30	0.1918	-0.067	-0.53	-0.46
84	10	0.50	0.1	10	0.01	45	0.2	-0.029	-1.20	-1.18

Table 5 – Runs having lateral shift to the drive side

Most of the runs have the thick section at its extreme value (0.5 mm) oriented against the downstream roller (~z=0.2), with the longest span length and higher modulus.

Wrinkled Web

Simulation runs 45, 65, and 81 resulted in significant wrinkling of the web and so were not included in the lateral shift plots. The change in width from upstream to downstream roller, Δw, is an indicator of wrinkling as the average change in width in the simulation (minus these runs) was only -0.0125 mm.

Run	s	t	E_s	L/W	ε_{md}	y	z	Δw
45	45	0.44	0.6	1	0.02	27.5	0.17	-1.32
65	50	0.50	0.2	10	0.019	0	-0.2	0.47
81	50	0.50	1.0	6.7	0.018	0	-0.198	0.83

Table 6 – Wrinkled web indicated by change in width from upstream to downstream roller

These runs have higher strain, the thick section close to or on the centerline of the base web, and the thickness biased to the extreme toward or away from the roller.

Run 8 (Δw= 0.02 mm), exhibited a small wrinkle but was included in the plots:

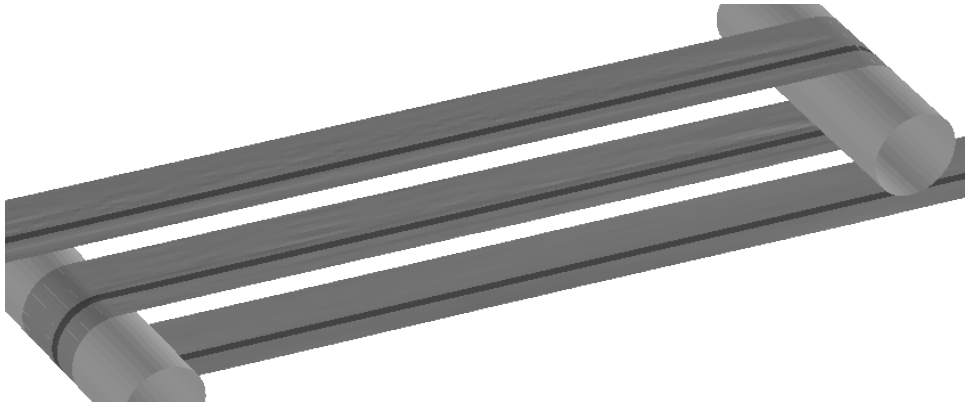

Figure 16 – Run 8 wrinkle simulation result

DISCUSSION

A traveling uniform web approaches a roller perpendicularly to the roller axis [4]. In this simulation, the web's inhomogeneity from having a thick section located at different CMD locations and z-plane offsets induces steering moments similar to those induced by cambered webs and tapered rollers.

Two sources of the steering moments include the **local velocity increase on the roller and the local stiffness increase due to the thick section**. For both cases, generally the steering effect is increased when the thick section is closer to the web edge.

The local velocity increase at the location of the thick section of the web is due to the section's larger pitch line radius. This larger velocity relative to the base web velocity induces a moment that causes bending stresses in the web and to achieve normal entry at the downstream roller the web moves laterally.

If the thick section is located on the base web centerline, the larger velocity in the center of the web causes stress that induce the web edges to move in towards the center, similar to the effect of a crowned roller. Larger thickness sections positioned closer to the web edge increase the moment induced and the compensating lateral shift to achieve normal entry, similar to the spreading effect induced by a concave or stepped roller.

The local increase in stiffness is due both to the increased thickness and any localized section modulus difference. Real manufacturing processes may create localized material differences via manufacturing process variability or by design. This increased stiffness induces a force profile different from a uniform web.

Factors that interact with the bending stresses are the span length/width ratio and the strain. Higher average strain stiffens the web, reducing the in-plane bending induced by the thick section, reducing the associated lateral shift. Longer span lengths generally make for a longer beam and so moments induce bending more easily.

CONCLUSIONS

There is a complex relationship between the web and process for an inhomogeneous web and its influence on web lateral dynamics and wrinkling. The finite element method enables analysis of a wide range of possible inhomogeneities. For the case of a web containing a section of increased thickness or stiffness there may exist a specific combination of average strain and span length to reduce its steering or wrinkling effect.

REFERENCES

1. Biesel, J. A., "Single Span Web Buckling Due to Roller Imperfections in Web Process Machinery," Ph.D. Dissertation, January 2007, Oklahoma State University, USA.
2. Beisel, J. A. and Good, J. K., "Analysis of Trough Formation and Lateral Steering of a Web Due to a Tapered Downstream Roller," Proceedings of the Eighth International Conference on Web Handling, Oklahoma State University, USA, June 5-8, 2005, pp. 81-97.
3. Good, J. K., Beisel, J. A., and Yurtcu, H., "Predicting Web Wrinkles on Rollers," Proceedings of the Tenth International Conference on Web Handling, Oklahoma State University, USA, June 7-10, 2009, pp. 495-530.
4. Shelton, J. J., "Lateral Dynamics of a Moving Web," PhD Thesis, Oklahoma State University, July, 1968.

5. Swanson, R. P., "Lateral Dynamics of Non-Uniform Webs," Proceedings of the Tenth International Conference on Web Handling, Oklahoma State University, USA, June 7-10, 2009, pp. 531-554.

APPENDIX

Table 7 – Simulation variables and output data

Run	s (mm)	t (mm)	E_s (GPa)	L/W	ε_{md}	y (mm)	z (mm)	Δw (mm)	d_{op} (mm)	d_{dr} (mm)
1	35	0.14	0.1	4.7	0.011	22.5	0.00088	0.000755	0.0768	0.076045
2	5	0.13	0.5	5	0.005	17.5	0.006675	-0.0067262	-0.0205	-0.0137738
3	10	0.19	0.3	1.8	0.01	5	-0.045	0.01701	0.0301	0.01309
4	40	0.17	0.9	1	0.008	10	-0.03402	-0.005215	0.0008	0.006015
5	50	0.10	0.1	6.3	0.017	0	0	0.000891	0.0003	-0.000591
6	30	0.10	0.1	10	0.008	0	0	-0.000201	-0.0004	-0.000199
7	20	0.41	0.1	1	0.02	10	-0.155	-0.058875	-0.0275	0.031375
8	10	0.50	0.9	8.2	0.007	15	-0.2	0.019236	1.5901	1.570864
9	20	0.50	0.1	9	0.005	0	0.2	-0.002655	-0.0908	-0.088145
10	45	0.10	1.0	3.2	0.015	27.5	0	-0.001201	-0.0484	-0.047199
11	40	0.46	0.8	1	0.005	0	0.12492	0.0010286	-0.0005	-0.0015286
12	40	0.50	0.4	8.7	0.005	25	-0.1494	0.0278089	2.3078	2.2799911
13	40	0.32	0.1	1	0.005	10	0.10307	-0.0074136	0.0081	0.0155136
14	20	0.10	1.0	9.9	0.02	0	0	0.002012	0.0014	-0.000612
15	10	0.49	0.8	2.1	0.02	35	-0.127335	0.029788	0.24	0.210212
16	40	0.25	0.6	10	0.013	5	-0.075	0.007365	0.0535	0.046135
17	20	0.45	1.0	10	0.02	0	-0.11935	-0.07615	0.3838	0.45995
18	50	0.34	1.0	9.8	0.011	25	-0.12	-0.036569	0.3417	0.378269
19	30	0.50	0.9	9.5	0.019	5	0.1994	-0.18558	-0.7695	-0.58392
20	40	0.50	0.5	10	0.02	30	-0.1258	0.026482	0.5549	0.528418
21	40	0.50	1.0	10	0.02	30	0.2	-0.142324	-1.8376	-1.695276
22	5	0.49	0.5	5.5	0.02	47.5	0.19344	0.015152	1.789	1.773848
23	50	0.50	1.0	1.9	0.005	0	-0.2	0.0151513	0.0086	-0.0065513
24	10	0.50	0.1	1.2	0.005	0	0.0774	-0.0035986	-0.0032	0.0003986
25	50	0.10	0.1	9.9	0.005	25	0	0.0001072	0.0003	0.0001928
26	10	0.10	0.6	1	0.017	35	0	-0.000822	-0.0063	-0.005478
27	5	0.10	1.0	1.4	0.005	37.5	0	-0.0010837	-0.0061	-0.0050163
28	10	0.30	1.0	2.2	0.005	0	-0.0383	0.0042403	0.003	-0.0012403
29	50	0.27	0.1	1	0.005	25	-0.08347	-0.0059395	0.0399	0.0458395
30	50	0.14	0.1	1.1	0.02	25	0.01876	-0.002448	0.0153	0.017748
31	10	0.10	0.1	1	0.005	45	0	-0.0113123	-0.0056	0.0057123

Run	s (mm)	t (mm)	E_s (GPa)	L/W	ε_{md}	y (mm)	z (mm)	Δw (mm)	d_{op} (mm)	d_{dr} (mm)
32	10	0.29	0.1	8.4	0.018	0	-0.095	-0.064807	-0.0164	0.048407
33	50	0.13	1.0	4.6	0.019	0	-0.015	0.002922	0.0023	-0.000622
34	20	0.50	1.0	10	0.005	0	0.1396	-0.0282811	-0.0799	-0.0516189
35	50	0.10	0.1	2.2	0.005	0	0	-0.0008215	-0.0006	0.0002215
36	50	0.14	0.3	7.1	0.005	0	0.02	-0.0042284	-0.0016	0.0026284
37	10	0.10	0.2	10	0.02	45	0	-0.004274	-0.0038	0.000474
38	50	0.10	0.3	1	0.02	20	0	-0.00676	-0.0066	0.00016
39	5	0.22	0.9	10	0.012	32.5	0.06	-0.017651	-0.8561	-0.838449
40	10	0.50	0.1	10	0.02	25	-0.0188	-0.002278	0.6245	0.626778
41	50	0.10	0.9	10	0.02	15	0	0.005224	-0.0212	-0.026424
42	25	0.24	1.0	5.7	0.02	37.5	0.0266	0.013608	0.4359	0.422292
43	50	0.50	0.8	5.8	0.012	15	0.0332	0.004062	0.2143	0.210238
44	40	0.50	0.1	10	0.02	0	0.1602	-0.028666	-0.0824	-0.053734
45	45	0.44	0.6	1	0.02	27.5	0.17	-1.323696	-0.3034	1.020296
46	50	0.44	1.0	1	0.005	25	0.17	0.0002301	0.0435	0.0432699
47	50	0.50	0.1	1.9	0.01	25	0.1168	-0.02273	0.2325	0.25523
48	50	0.10	0.4	1	0.005	25	0	-0.0079865	-0.0042	0.0037865
49	10	0.10	0.1	10	0.006	45	0	-0.0019908	-0.0014	0.0005908
50	10	0.22	0.1	2.7	0.019	45	-0.01866	-0.015726	0.0772	0.092926
51	10	0.10	0.8	8.6	0.005	0	0	-3.52E-05	0.0008	0.0008352
52	30	0.50	0.8	1	0.015	0	-0.1804	0.034657	0.0033	-0.031357
53	50	0.10	1.0	7.8	0.005	0	0	0.0017757	0.0013	-0.0004757
54	30	0.10	0.1	1	0.018	0	0	-0.001842	-0.001	0.000842
55	50	0.48	1.0	1.6	0.005	25	-0.19	0.0120079	0.0264	0.0143921
56	10	0.50	0.8	4.1	0.005	30	0.1918	-0.0673681	-0.533	-0.4656319
57	50	0.42	0.3	1	0.011	5	-0.10576	-0.024896	-0.0046	0.020296
58	50	0.10	1.0	6.6	0.02	0	0	0.002553	0.0015	-0.001053
59	5	0.50	1.0	1.1	0.018	17.5	0.2	-0.081596	-0.0172	0.064396
60	10	0.50	0.5	1	0.005	20	-0.2	-0.0051102	0.0303	0.0354102
61	50	0.37	0.1	10	0.01	10	0.02349	-0.020634	0.0246	0.045234
62	50	0.10	0.1	10	0.02	0	0	0.000343	0.0004	5.7E-05
63	10	0.10	0.9	1	0.02	35	0	-0.007744	-0.0199	-0.012156
64	50	0.50	0.8	10	0.005	0	-0.1268	0.004792	0.0918	0.087008
65	50	0.50	0.2	10	0.019	0	-0.2	-0.458283	0.0096	0.467883
66	50	0.10	0.5	1	0.014	5	0	0.004192	0.0017	-0.002492
67	15	0.43	1.0	10	0.005	42.5	0	0.06796	7.486	7.41804
68	40	0.50	0.4	1	0.015	30	-0.2	-0.0457959	0.0782	0.1239959

Run	s (mm)	t (mm)	E_s (GPa)	L/W	ε_{md}	y (mm)	z (mm)	Δw (mm)	d_{op} (mm)	d_{dr} (mm)
69	30	0.10	0.9	10	0.005	0	0	0.0010199	0.0002	-0.0008199
70	5	0.50	0.1	1	0.02	12.5	0.1966	-0.019599	-0.0247	-0.005101
71	50	0.10	0.6	10	0.005	20	0	0.0002759	-0.0121	-0.0123759
72	10	0.41	0.5	5.9	0.013	0	0.041695	-0.009179	-0.0128	-0.003621
73	15	0.22	0.6	7.3	0.01	42.5	-0.05994	0.020328	0.9272	0.906872
74	30	0.23	1.0	1	0.02	10	0.019175	-0.015114	-0.0025	0.012614
75	35	0.38	0.5	7.2	0.005	32.5	0.14	0.0246488	3.096	3.0713512
76	10	0.50	0.1	1	0.01	45	0.2	-0.008014	0.0539	0.061914
77	50	0.17	0.7	10	0.013	15	0.035	-0.005959	0.0047	0.010659
78	10	0.10	0.1	10	0.02	0	0	0.000343	0.0004	5.7E-05
79	5	0.14	1.0	10	0.02	32.5	-0.01602	0.002141	-0.0546	-0.056741
80	50	0.50	1.0	2.3	0.017	0	0.2	-0.054536	0.0155	0.070036
81	50	0.50	1.0	6.7	0.018	0	-0.198	-0.871675	-0.0405	0.831175
82	50	0.46	0.1	1	0.019	0	0.18	-0.039559	-0.0039	0.035659
83	40	0.15	1.0	3.8	0.005	15	0.01985	-0.0069435	0.0177	0.0246435
84	10	0.50	0.1	10	0.01	45	0.2	-0.029012	-1.205	-1.175988
85	50	0.26	0.1	10	0.013	25	-0.08	-0.009971	0.9974	1.007371
86	30	0.26	0.4	5.7	0.02	15	0.08	-0.071447	0.0465	0.117947
87	30	0.31	0.7	1	0.008	30	-0.00063	-0.002009	0.0186	0.020609
88	30	0.50	0.1	7.2	0.007	0	-0.2	-0.0296099	-0.021	0.0086099
89	50	0.38	0.1	5.1	0.02	15	-0.0364	-0.00564	0.397	0.40264
90	20	0.10	1.0	1	0.01	0	0	0.001703	0.0009	-0.000803
91	5	0.36	0.2	10	0.005	22.5	-0.04082	0.0027483	0.6594	0.6566517
92	30	0.10	0.3	8.3	0.02	25	0	0.002414	-0.0909	-0.093314
93	10	0.10	0.7	5.1	0.02	0	0	0.000779	0.0006	-0.000179
94	10	0.49	1.0	10	0.016	45	-0.195	0.030098	2.1865	2.156402
95	50	0.41	1.0	1	0.02	15	-0.126325	-0.06711	-0.0645	0.00261
96	50	0.38	1.0	8.1	0.008	0	0.14	-0.022146	0.0038	0.025946
97	50	0.50	0.2	9.4	0.017	25	0.2	-0.234717	2.5259	2.760617
98	50	0.10	1.0	1	0.018	25	0	-0.003421	-0.0073	-0.003879
99	5	0.10	1.0	2.1	0.005	47.5	0	-0.0008612	-0.0111	-0.0102388
100	5	0.50	0.1	5.4	0.011	47.5	-0.1618	0.026437	0.9009	0.874463